Electrochemical State Observer Design for Li-Ion Batteries With Heterogenous Electrode Lithiation

Mian Mohammad Arsalan Asif, Federico Bribiesca-Argomedo

Electrochemical State Observer Design for Li-Ion Batteries With Heterogenous Electrode Lithiation

Mian Mohammad Arsalan Asif and Federico Bribiesca-Argomedo

***Abstract*—Real-time reconstruction of electrochemical state information is essential for high-fidelity monitoring and high-performance operation in advanced battery management systems. In this letter, a Partial Differential Equation (PDE) based observer is developed for a simplified Doyle-Fuller-Newman electrochemical model of a Li-ion battery. This observer enables the reconstruction of the internal states of the battery based on current and voltage measurements while also exploring the impact of including new sensor technologies in the battery cell. In particular, the exploitation of reference electrode and fiber-optic sensors is considered. Stability analysis of the observer components is done using Lyapunov techniques, their effectiveness in spatially tracking the electrochemical states of the original system is demonstrated through simulation results, and robustness to noise in input is analyzed.**

***Index Terms*—Distributed parameter systems, observers for nonlinear systems, stability of nonlinear systems.**

I. Introduction

In RECENT years, a significant growth in the demand for Lithium-ion batteries (LiBs) has made control system technologies that enhance their performance, an active research topic [1]. Different modeling approaches have emerged that include Equivalent Circuit Models (ECMs), Machine Learning (ML), and Electrochemical models (EChMs).

ECMs offer a computationally cheap way to mimic battery input-output behavior but provide limited information on the internal behavior of the battery. Comprehensive reviews of ECMs, highlighting their applications and limitations, can be found in the literature, e.g., [2]. ML tools have been employed to identify battery models using sensor data [3]. However, these models require extensive training data for parameters and electrochemical properties that can vary drastically.

EChMs provide a deeper understanding of the internal states of the battery by considering the electrochemical processes occurring within the battery. The Doyle-Fuller-Newman (DFN) model [4] is a widely recognized and reliable EChM for LiBs. However, due to its complexity, researchers have sought simpler alternatives that can still provide accurate estimations [5], [6], [7]. Recently hybrids between ML and EChM have also been proposed [8]. A comparative review of the aforementioned strategies is presented in [9], [10], [11], [12].

In this letter, we intend to tackle two challenges faced by these strategies in observing battery behavior. 1) The effectiveness and fidelity of LiB models decrease as it ages since many parameters can change acutely with the battery's state-of-health (SoH). Research on aging-aware modeling has emerged, coupling EChMs [13] or ECMs [14] with aging or degradation mechanisms intrinsic to LiBs. However, these methods are limited by the assumption of a known initial capacity in the electrolyte and electrodes. 2) The lack of observability of individual electrode states from measured terminal voltage [15]. This makes it difficult to reconstruct the internal states of the LiB on a spatial level.

These challenges have led to an increased focus on the development of novel sensor technologies, including reference electrodes that measure a reference voltage $V_{ref}(t)$ and sensors for lithium concentration in the electrolyte [16], [17], [18], [19], [20]. These sensors could provide the ability to obtain electrode-level information that can give several advantages over cell-level-only information, such as real-time monitoring for precise and safe battery control, identification of individual electrode contribution to degradation modes, and insights into better electrode design [21]. Existing techniques to obtain electrode-level information include an uncertain model-based estimation [22], and an ECM-based state of charge (SOC) estimation approach [23]. However, these techniques offer limited insight into the internal states of the LiBs.

A. Main Contributions

We propose two PDE-based observers for the estimation of solid and electrolyte lithium concentrations inside a cell based on a simplified DFN Model. The observers track the total lithium concentration in both the solid electrodes and in the electrolyte independently using a reference electrode and an electrolyte lithium concentration sensor. Their combination allows us to spatially reconstruct the internal states of the LiB, without assuming the correct initial knowledge of the amount of lithium in each phase. This approach does

Manuscript received 9 May 2023; revised 13 July 2023; accepted 3 August 2023. Date of publication 10 August 2023; date of current version 28 August 2023. This work was supported by the European Union's Horizon 2020 Research and Innovation Program under Grant 955930. Recommended by Senior Editor C. Prieur. *(Corresponding author: Mian Mohammad Arsalan Asif.)*

The authors are with Univ. Lyon, INSA Lyon, Université Claude Bernard Lyon 1, Ecole Centrale de Lyon, CNRS, Ampère, UMR5005, 69621 Villeurbanne, France (e-mail: mmarsalan94@gmail.com).

Digital Object Identifier 10.1109/LCSYS.2023.3304248

not require inverting the OCV (Open Circuit Voltage) curves, unlike other approaches (e.g., [5]). The independent stability of these observers is proven using a Lyapunov approach and their effectiveness, once interconnected, is demonstrated with simulation results. The robustness of the observers with respect to measurement noise is then analyzed.

II. Model

The DFN equations [4] model 1D LiB behavior by considering two phases: the (liquid) electrolyte, and the (solid) electrodes. The time-evolution of concentration in the electrodes $c_s^{\pm}$ and electrolyte c_e is represented by the diffusion equations:

$$c^{\pm}_{s,t}(x,r,t) = \frac{1}{r^2}\frac{\partial}{\partial r}\Big[D_s^{\pm} r^2 c^{\pm}_{s,r}(x,r,t)\Big] \tag{1}$$

$$\epsilon_e^j c^j_{e,t}(x,t) = \frac{\partial}{\partial x}\left[D_e(c_e^j)c^j_{e,x} + \frac{(1-t_c^0)}{F} i_e^j(x,t)\right] \tag{2}$$

for $j \in \{-, sep, +\}$ where D_e is the effective electrolyte diffusivity given by the Bruggeman relationship or other models and subindexes r, t, x denote the partial derivative with respect to the particular variable. The boundary conditions for the diffusion equations are:

$$\begin{aligned} 2c^{\pm}_{s,r}(x,0,t) &= 0, \qquad & c^{\pm}_{s,r}(x,R_s^{\pm},t) &= \frac{-j_n^{\pm}(x,t)}{D_s^{\pm}} \\ \Psi^-(0,t) &= 0, & \Psi^+(L^T,t) &= 0 \qquad (3) \\ c_e(l^-,t) &= c_e(0^{sep},t), & c_e(l^{sep},t) &= c_e(0^+,t), \\ \Psi^-(l^-) &= \Psi^{sep}(0^{sep}), & \Psi^{sep}(l^{sep}) &= \Psi^+(0^+), \qquad (4) \end{aligned}$$

where $\Psi^j(x) = D_e^j(c_e(x))c^j_{e,x}(x,t)$. The diffusion equations are dependent upon the governing equations:

$$\begin{aligned} \sigma^{eff,\pm}\phi^{\pm}_{s,x}(x,t) &= i_e^{\pm} - I(t), \quad i^{\pm}_{e,x}(x,t) = a^{\pm}F j_n^{\pm}(x,t), \\ j_n^{\pm}(x,t) &= \frac{i_0^{\pm}(x,t)}{F}\left[e^{\frac{\alpha_a F}{RT}\eta^{\pm}(x,t)} - e^{\frac{(1-\alpha_a)F}{RT}\eta^{\pm}(x,t)}\right], \\ \kappa^{eff}(c_e)\phi_{e,x}(x,t) &= -i_e^{\pm} + \kappa^{eff}(c_e)\frac{2RT}{F}(1-t_c^0)d_1\frac{\partial}{\partial x}\ln c_e(x,t), \\ \eta^{\pm}(x,t) + \phi_e(x,t) &= \phi_s^{\pm}(x,t) - U^{\pm}(c_{ss}^{\pm}(x,t)) - FR_f^- j_n^-(x^-,t). \end{aligned} \tag{5}$$

Description of the variables is given in Tab. I. The input to the model is the applied current density $I(t)[A/m^2]$ and the output voltage measured across the current collectors is given by $V(t) = \phi_s^+(L^T,t) - \phi_s^-(0,t)$. The voltage measured from the negative collector to the reference electrode is given by $V_{ref}(t) = \phi_e(x^r,t) - \phi_s^-(0,t)$. The potential differences through the model are shown in Figure 1. More complete detail of the DFN model is given in [4].

III. State Observer Design

In this section, we will discuss the construction and stability analysis of the state observer for 1) c_e in the electrolyte, and 2) $c_s^{\pm}$ in the electrode domains, including new measurements available from a reference electrode and a potential Li concentration sensor.

A. State Observer for the Electrolyte Lithium Concentration

The electrolyte observer is derived under the following assumptions:

TABLE I
Description of Variables in the Governing Equations

Variable	Description	Variable	Description
$\phi_e(x,t)$	Electrolyte potential	$\phi_s^{\pm}(x,t)$	Solid potential
$\kappa^{eff}(c_e)$	Effective electrolyte conductivity	$i_e^{\pm}(x,t)$	Ionic current
$\sigma^{eff,\pm}$	Effective solid conductivity	$j_n^{\pm}(x,t)$	Ionic fluxes
$R_f^{\pm}$	Interphase film resistance	$\eta^{\pm}(x,t)$	Overpotential
$f_{c/a}$	Mean molar activity coefficient	d_1	$1 + \frac{d\ln f_{c/a}}{d\ln c_e}$
$a^{\pm}$	Interfacial surface area	F	Faraday const.
R	Universal gas constant	T	Temperature
α_a	Anodic charge transfer coefficient	$i_0^{\pm}$	Exchange current density

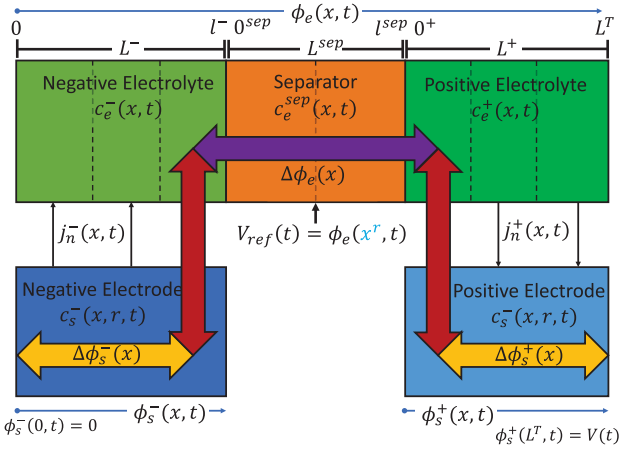

Fig. 1. Potentials inside the battery.

Assumption 1: D_e is uniformly bounded such that there exist positive $\underline{D}_e$ and $\overline{D}_e$ such that $\forall\ c_e^j, \overline{D}_e \geq D_e(c_e^j) \geq \underline{D}_e > 0$. This will allow us to consider D_e as a function of x and t in our proofs.

Assumption 2: A measurement of the lithium concentration in the electrolyte $c_e(x^r,t)$ at a specific point in the separator x^r is available.

Assumption 3: The spatial profile of molar ionic fluxes $j_n^{\pm}(x,t)$ is assumed to be adequately predicted by the model without correction. Therefore the ionic current $i_e^{\pm}(x,t)$ profile is assumed to be known. This allows us to consider the stability of the electrolyte observer independently of that of the electrode observer. This is a limitation of the current design since the stability of the interconnection is only shown in simulation results. This shortcoming is shared by other approaches which require similar assumptions, e.g., [5].

By utilizing the electrolyte diffusion equation of the DFN model (2) under Assumption 1, a simplified expression of the electrolyte diffusion equation is derived:

$$\epsilon_e^j c^j_{e,t}(x,t) = \frac{\partial}{\partial x}\left[D_e(x,t)c^j_{e,x}(x,t) + \frac{(1-t_c^0)}{F} i_e^j(x,t)\right] \tag{6}$$

with analogous boundary conditions. Using Assumption 2, the electrolyte concentration observer is formulated by including an error injection term in the diffusion equation:

$$\begin{aligned} \epsilon_e^j \hat{c}^j_{e,t}(x,t) = \frac{\partial}{\partial x}\left[D_e(x,t)\hat{c}^j_{e,x}(x,t) + \frac{1-t_c^0}{F} i_e^j(x,t)\right] \\ - P\big[c_e(x^r,t) - \hat{c}_e(x^r,t)\big] \end{aligned} \tag{7}$$

with $x^r \in [0^{sep}, l^{sep}]$. The error system can be formulated as the difference between the physical system represented by (2)

and the observer system in (7) with $u(x) \doteq c_e(x,t) - \hat{c}_e(x,t)$. Under Assumption 1 and 2, the diffusion equation of the error system can be expressed as:

$$\epsilon_e^j u_t(x) = [D_e(x)u_x(x)]_x + Pu(x^r) \tag{8}$$

with analogous boundary conditions to the original system (4). Due to space restrictions, the time dependence of the variable $u(x)$ and $D_e(x)$ is dropped. Although, it should be kept in mind these variables and their derivatives are indeed time-dependent.

Proposition 1: $\forall P < 0$, the origin of the error system in (8) is exponentially stable in the $H_1(0, L^T)$ norm if Assumptions 1 - 3 hold.

Proof: Let us define a candidate Lyapunov function $V_T = V_1 + \beta V_2$ with $V_1(u(\cdot,t)) \doteq \frac{1}{2}\int_0^{L^T} \epsilon_e u^2(x)dx$, and $V_2(u(\cdot,t)) \doteq \frac{1}{2}\int_0^{L^T}[\epsilon_e D_e(x)u_x^2(x)]dx$, where ϵ_e varies within the regions $\{-, sep, +\}$, and β is chosen later. By differentiating V_1 with respect to time and using the error system equations, the time derivative is obtained:

$$\dot{V}_1 = \int_0^{L^T} \epsilon_e u_t(x)u(x)dx$$

By substituting Equation (8) into the integral on the right-hand side of the equation, we obtain:

$$\dot{V}_1 = \int_0^{L^T} \frac{\partial}{\partial x}[D_e(x)u_x(x)]u(x)dx + \int_0^{L^T} Pu(x^r)u(x)dx \tag{9}$$

Integration by parts on the first term on the right-hand side can be performed to give:

$$\begin{aligned}\dot{V}_1 &= -\int_0^{L^T} D_e(x)u_x^2(x)dx + \int_0^{L^T} Pu(x^r)u(x)dx \\ &\leq -\underline{D}_e\left[\int_0^{x^r} u_x^2(x)dx + \int_{x^r}^{L^T} u_x^2(x)dx\right] + \int_0^{L^T} Pu(x^r)u(x)dx\end{aligned}$$

Lets us now define for the negative domain, the following relationship through integration by parts:

$$\int_0^{x^r} u^2(x)dx = u^2(x^r)x^r - 2\int_0^{x^r} xu(x)u_x(x)dx$$

Using Young's Inequality, the right-hand side of the equation becomes:

$$\begin{aligned}\int_0^{x^r} u^2(x)dx &\leq u^2(x^r)x^r + A_1\int_0^{x^r} xu^2(x)dx + \frac{1}{A_1}\int_0^{x^r} xu_x^2(x)dx \\ &\leq x^r\left[u^2(x^r) + A_1\int_0^{x^r} u^2(x)dx + \frac{1}{A_1}\int_0^{x^r} u_x^2(x)dx\right]\end{aligned}$$

for any $A_1 > 0$. Rearranging the above inequality and writing $x^r \leq M_A$ where $M_A = \max\{x^r, L^T - x^r\}$ yields:

$$-\int_0^{x^r} u_x^2(x)dx \leq A_1 u^2(x^r) + \frac{A_1^2 M_A - A_1}{M_A}\int_0^{x^r} u^2(x)dx \tag{10}$$

Following a similar process on the positive domain yields:

$$-\int_{x^r}^{L^T} u_x^2 dx \leq A_2 u^2(x^r) + \frac{A_2^2(M_A) - A_2}{M_A}\int_{x^r}^{L^T} u^2 dx \tag{11}$$

for any $A_2 > 0$. Now adding (10) and (11), defining $A \doteq A_1 = A_2 > 0$, and then rearranging the inequality yields

$$-\int_0^{L^T} u_x^2 dx \leq -\left[\frac{A - A^2 M_A}{M_A}\right]\int_0^{L^T} u^2 dx + 2Au^2(x^r) \tag{12}$$

We choose $A \in (0, 1/M_A)$ to ensure that $(A - A^2 M_A) > 0$. By utilizing equation (12) with $V_1(t) \leq (\bar{\epsilon}_e/2)\int_0^{L^T} u^2(x)dx$, the resulting expression for $\dot{V}_1$ is:

$$\begin{aligned}\dot{V}_1 &\leq -\underline{D}_e\kappa_A\int_0^{L^T} u^2(x)dx + 2\underline{D}_e A u^2(x^r) + \int_0^{L^T} Pu(x^r)u(x)dx \\ &\leq -\frac{2\underline{D}_e}{\bar{\epsilon}_e}\kappa_A V_1 + 2\underline{D}_e A u^2(x^r) + \int_0^{L^T} Pu(x^r)u(x)dx\end{aligned}$$

where $\kappa_A = (A - A^2 M_A)/M_A$, and $\bar{\epsilon}_e$ is the maximum value of ϵ_e. Using the following relationships:

$$\begin{aligned}\int_{x^r}^{L^T} Pu(x^r)u(x)dx &= Pu(x^r)\left[[L^T - x^r]u(x^r) + \int_{x^r}^{L^T}\int_{x^r}^{x} u_x(s)dsdx\right] \\ \int_0^{x^r} Pu(x^r)u(x)dx &= Pu(x^r)\left[x^r u(x^r) + \int_0^{x^r}\int_{x^r}^{x} u_x(s)dsdx\right]\end{aligned}$$

on the last term on the right-hand side of the inequality, therefore

$$\begin{aligned}\dot{V}_1 \leq -\frac{2\underline{D}_e}{\bar{\epsilon}_e}\kappa_A V_1 + 2\underline{D}_e A u^2(x^r) + Pu^2(x^r)(L^T) \\ + \int_0^{L^T} Pu(x^r)\int_{x^r}^{x} u_x(s)dsdx\end{aligned}$$

Using Young's and Cauchy-Schwarz Inequalities on the fourth term of the right-hand side, we obtain

$$\begin{aligned}\dot{V}_1 \leq -\frac{2\underline{D}_e}{\bar{\epsilon}_e}\kappa_A V_1(t) + \frac{L^T}{2\gamma}|x - x^r|\int_{\min\{x^r,x\}}^{\max\{x^r,x\}} u_x^2(s)ds \\ + u^2(x^r)\left[2\underline{D}_e A + PL^T + \frac{P^2 L^T}{2}\gamma\right]\end{aligned}$$

where $\gamma > 0$. We now bound the integral and absolute coefficient of the second term on the right-hand side with the interval $[0, L^T]$ to obtain

$$\begin{aligned}\dot{V}_1 \leq -\frac{2\underline{D}_e}{\bar{\epsilon}_e}\kappa_A V_1(t) + \frac{(L^T)^2}{2\gamma}\int_0^{L^T} u_x^2(x)dx \\ + u^2(x^r)\left[2\underline{D}_e A + PL^T + \frac{P^2 L^T}{2}\gamma\right]\end{aligned}$$

We now differentiate V_2 with respect to time and utilize the expression in (8) to obtain:

$$\dot{V}_2 = \int_0^{L^T} (D_e(x)u_x(x)[D_e(x)u_x(x)]_{xx})dx$$

Integration by parts on the right-hand side can be performed to yield:

$$\dot{V}_2 = -\int_0^{L^T} \frac{\partial}{\partial x}[D_e(x)u_x(x)]^2 dx$$

Utilizing Poincare's Inequality, writing the term on the right-hand side of the inequality as the sum of two elements, and introducing the inequality $V_2(t) \leq (\bar{\epsilon}_e/2)\int_0^{L^T} D_e(x)u_x^2 dx$, allows us to rewrite the above inequality as

$$\dot{V}_2 \leq -\frac{\alpha}{4L^{T^2}}\underline{D}_e^2\int_0^{L^T} u_x^2(x)dx - \frac{1-\alpha}{2\bar{\epsilon}_e L^{T^2}}\underline{D}_e V_2$$

where $0 < \alpha < 1$. We can now write the Lyapunov function $V_T = V_1(t) + \beta V_2(t)$ and differentiate to obtain

$$\dot{V}_T(t) \leq -\frac{\underline{D}_e}{\bar{\epsilon}_e} \min\left\{2\kappa_A, \frac{1-\alpha}{2\bar{L}^{T2}}\right\} V_T(t) + \left[\frac{L^{T2}}{2\gamma} - \frac{\alpha \underline{D}_e^2}{4L^{T2}}\beta\right] \times \int_0^{L^T} u_x^2(x)dx + u^2(x^r)\left[2\underline{D}_e A + PL^T + \frac{P^2 L^T}{2}\gamma\right]$$

In order to guarantee the exponential stability of the solution, it is necessary to satisfy the following constraints:

$$2L^{T4} - \alpha \underline{D}_e^2 \beta\gamma \leq 0, 4\underline{D}_e A + 2P\,L^T + P^2 L^T \gamma \leq 0. \quad (13)$$

With the choice of parameters:

$$\gamma = -\frac{1}{P}, 0 < A \leq \min\left\{\frac{L^T}{4\gamma \underline{D}_e}, \frac{1}{M_A}\right\}, \beta \geq \frac{2(L^T)^4}{\gamma\alpha \underline{D}_e^2},$$

the constraints in (13) are satisfied. This proves the exponential stability of the electrolyte state observer system. ■

B. State Observer for the Solid Lithium Concentration Using Voltage Error Injection

We will now discuss the construction of state observers for the solid electrodes with the use of voltage available at the reference electrode. We introduce the following assumptions:

Assumption 4: A voltage measurement at a reference electrode $V_{ref}(t)$ is available. This allows for independent estimations of OCV potentials $U^{\pm}$ for each electrode.

Assumption 5: The OCV curve of the electrodes $U^{\pm}$ is assumed to be strictly monotonically decreasing (uniformly in the concentration) in such a way that, defining $f(a,b) \doteq U(a) - U(a-b)$, the following property is satisfied:

$$\exists k_1, k_2 < 0 \text{ s.t. } \forall a, b \qquad k_1 b^2 \leq f(a,b)b \leq k_2 b^2 \quad (14)$$

Note that the proofs can be adapted without problem if the function is monotonically increasing, requiring only a change of sign in the feedback gain.

Using Assumption 4, the solid-phase lithium concentration observer is formulated by injecting the voltage error term:

$$\begin{aligned}
\hat{c}_{s,t}^{\pm}(x,r,t) &= \frac{1}{r^2}\frac{\partial}{\partial r}\left[D_s^{\pm} r^2 \hat{c}_{s,r}^{\pm}\right] \\
\hat{c}_{s,r}^{\pm}(x,0,t) &= 0 \\
\hat{c}_{s,r}^{\pm}(x,R_s^-,t) &= -\frac{j_n^{\pm}(x,t)}{D_s^{\pm}} \\
&\quad - g_0^{\pm}\left[U(c_{ss}^{\pm}(x,t)) - U(\hat{c}_{ss}^{\pm}(x,t))\right] \quad (15)
\end{aligned}$$

where $c_{ss}^{\pm}(x,t) \doteq c_s^{\pm}(x, R_s^{\pm}, t)$. To arrive at this error injection term, at particular points $x^{\pm}$, the governing equations in (5) and Figure 1 are used to write:

$$\begin{aligned}
U(\hat{c}_{\text{ss}}^{-}(x^-,t)) &= -\hat{V}_{\text{ref}}(t) + \hat{\phi}_e(x^r,t) - \hat{\phi}_e(x^-,t) \\
&\quad - FR_f^- \hat{j}_n^-(x^-,t) - \hat{\eta}^-(x^-,t) + \hat{\phi}_s^-(x^-,t) \\
U(\hat{c}_{\text{ss}}^{+}(x^+,t)) &= \hat{V}(t) - \hat{V}_{\text{ref}}(t) - \hat{\phi}_e(x^+,t) + \hat{\phi}_e(x^r,t) - \hat{\phi}_s^+(L^T,t) \\
&\quad + \hat{\phi}_s^+(x^+,t) + FR_f^+ \hat{j}_n^+(x^+,t) + \hat{\eta}^+(x^+,t) \quad (16)
\end{aligned}$$

Assumption 3 implies in particular that $\phi_s^{\pm}$ and $j_n^{\pm}$ are identical in both the estimated and real systems, and since the electrolyte subsystem observer converges exponentially to the actual value, we approximate the terms necessary for the error injection term using the measured voltages as follows:

$$\begin{aligned}
U(c_{\text{ss}}^-(x^-,t)) - U(\hat{c}_{\text{ss}}^-(x^-,t)) &\approx V_{ref}(t) - \hat{V}_{ref}(t) \\
U(c_{\text{ss}}^+(x^+,t)) - U(\hat{c}_{\text{ss}}^+(x^+,t)) &\approx [V(t) - V_{ref}(t)] - [\hat{V}(t) - \hat{V}_{ref}(t)] \quad (17)
\end{aligned}$$

Let us define the error system as the physical system represented by (1) and (3) minus the observer system (15), once again using Assumption 3 to decouple the stability analysis of both observers:

$$\begin{aligned}
z_t(r,t) &= \frac{1}{r^2}\frac{\partial}{\partial r}\left[D_s r^2 z_r(r,t)\right] \\
z_r(R_s^{\pm},t) &= g_0\left[U(\bar{z}(R_s^{\pm},t)) - U(\hat{z}(R_s^{\pm},t))\right], z_r(0,t) = 0.
\end{aligned}$$

where $z(r,t) \doteq c_s^{\pm}(x,r,t) - \hat{c}_s^{\pm}(x,r,t)$, $\hat{z} \doteq \hat{c}_s^{\pm}(x,r,t)$, $\bar{z} \doteq c_s^{\pm}(x,r,t)$, and the dependence on x has been suppressed, due to space restrictions. Using Assumption 5, we can express the error system in a compact form as:

$$\begin{aligned}
z_t(r,t) &= \frac{1}{r^2}\frac{\partial}{\partial r}\left[D_s r^2 z_r(r,t)\right] \\
z_r(R_s^{\pm},t) &= g_0 f(\bar{z}(R_s^{\pm},t), z(R_s^{\pm},t)), z_r(0,t) = 0
\end{aligned}$$

The radial coordinates are now transformed via normalization with the scaled value of $R_s^{\pm}$ such that $\bar{r} = r/R_s^{\pm}$. The over-bar notation is dropped henceforth to reduce clutter, resulting in the final expression for the error system:

$$z_t(r,t) = \frac{1}{R_s^2 r^2}\frac{\partial}{\partial r}\left[D_s r^2 z_r(r,t)\right] \quad (18)$$

$$z_r(1,t) = R_s g_0 f(\bar{z}(1,t), z(1,t)), z_r(0,t) = 0 \quad (19)$$

Proposition 2: For $\alpha \in (0,1)$, let g_0 be chosen such that $0 < g_0 \leq -3/[2k_2\alpha R_s]$ with k_2 defined in Assumption 5, then the origin of the error system given by Equations (18)-(19) is exponentially stable in the $L^2(S)$ norm, where $S = \{r \in \mathbb{R}^3 | \; ||r|| \leq 1\}$ if Assumptions 3 - 5 hold.

Proof: Let us define a candidate Lyapunov function:

$$V_s = \frac{1}{2}\int_0^1 \frac{R_s^2}{D_s} r^2 z^2(r,t)dr$$

and compute the time derivative

$$\dot{V}_s = \int_0^1 \frac{\partial}{\partial r}\left[r^2 z_r(r,t)\right] z(r,t)dr$$

By expanding the right-hand side of the equation, utilizing the method of integration by parts, and substituting $z_r(1,t)$ with the expression in Equation (19), we obtain:

$$\dot{V}_s = z(1,t)R_s g_0 f(\bar{z}(1,t), z(1,t)) - \int_0^1 r^2 z_r{}^2(r,t)dr$$

Using the properties defined in Assumption 5, we are able to write:

$$\dot{V}_s \leq k_2 R_s g_0 z^2(1,t) - \int_0^1 r^2 z_r{}^2(r,t)dr$$

Since k_2 is negative, we define a strictly positive constant $k_s = -k_2 R_s g_0$ such that $g_0 > 0$. We then split the first term on the right-hand side of the inequality into two parts to obtain:

$$\dot{V}_s \leq k_s\left[-\alpha z^2(1,t) - (1-\alpha)z^2(1,t)\right] - \int_0^1 r^2 z_r{}^2(r,t)dr. \quad (20)$$

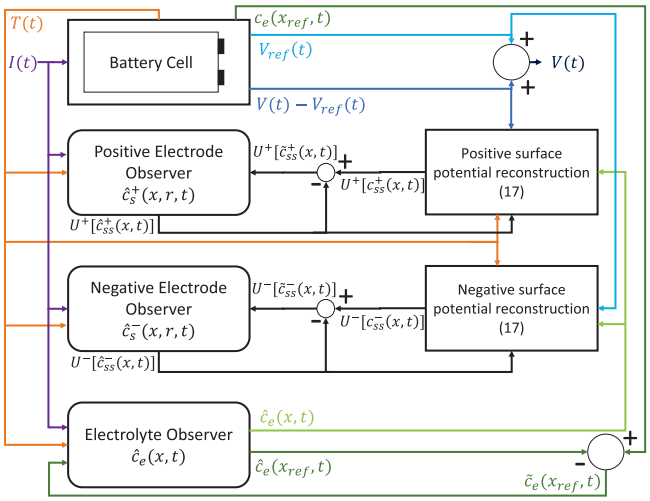

Fig. 2. Observer structure with voltage error injection.

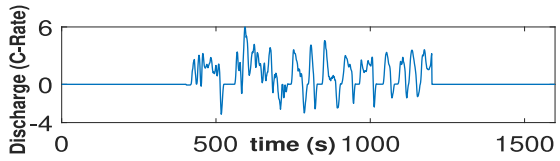

Fig. 3. Current profile of the UDDS cycle.

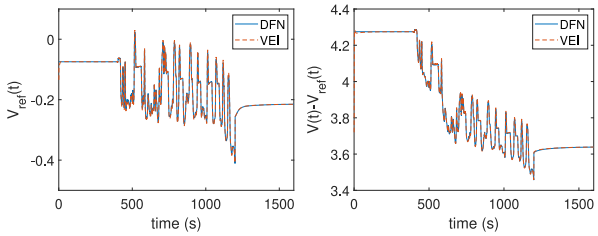

(b) $V_{ref}(t)$ (c) $V(t) - V_{ref}(t)$

Fig. 4. Voltages with the UDDS Cycle.

Let us now manipulate the term $-k_s\alpha z^2(1,t)$ through a change of variables:

$$w(r,t) = z(r,t)r \quad w_r(r,t) = z(r,t) + rz_r(r,t)$$

which allows us to write $-z^2(1,t) = -w^2(1,t)$. We can now use Poincare's Inequality to write

$$\begin{aligned} -z^2(1,t) &\leq -\frac{1}{2}\int_0^1 w^2(r,t)dr + 2\int_0^1 {w_r}^2(r,t)dr \\ &\leq -\frac{D_s}{R_s^2}V_s + 2\int_0^1 (z(r,t) + rz_r(r,t))^2 dr \end{aligned}$$

Through integration by parts, $\int_0^1 (2rz(r,t)z_r(r,t))dr = z^2(1,t) - \int_0^1 z^2(r,t)dr$, which allows us to write

$$-z^2(1,t) \leq -\frac{D_s V_s}{3R_s^2} + \frac{2}{3}\int_0^1 r^2 {z_r}^2(r,t)dr \qquad (21)$$

As the coefficient $k_s\alpha$ is strictly positive, we substitute the result of the inequality (21) into the main Lyapunov inequality (20), and combine common terms to write:

$$\dot{V}_s \leq -k_s\frac{\alpha D_s}{3R_s^2}V_s + \left[\frac{2k_s\alpha}{3} - 1\right]\int_0^1 r^2{z_r}^2(r,t)dr - (1-\alpha)k_s z^2(1,t)$$

With the choice of boundary gain $0 < g_0 \leq -3/[2k_2\alpha R_s]$, the time derivative of the candidate Lyapunov function is negative definite which proves the exponential stability of the electrode observers. Using the maximum value of g_0, we can further simplify the inequality to:

$$\dot{V}_s \leq -\frac{D_s}{2R_s^2}V_s - \frac{3(1-\alpha)}{2\alpha}z^2(1,t)$$

■

A feature of our proposed electrode observers is the estimation of the total amount of Lithium in the electrodes. They can be combined with a conservative observer like the one in [5], operating on different time-scales to errors in solid-phase lithium. The overall structure of the combined PDE-based observers for the electrolyte and electrode lithium concentrations is illustrated in Figure 2.

TABLE II
RMS ERROR OF THE VOLTAGES

error (mV)	$V(t)$	$V_{ref}(t)$	$V(t) - V_{ref}(t)$
VEI	5.4502	3.0438	2.8405
VEI (5mV noise)	6.9501	4.1694	4.2133
VEI (10mV noise)	10.0511	6.5705	6.7245

IV. Validation of Simulation Results

In this section, a comprehensive simulation analysis using a finite volume based simplified DFN model is conducted to evaluate the efficacy of the proposed observers for electrolyte and electrodes. To evaluate the performance of the two observers under varying operating conditions, the UDDS drive cycle which features a peak current of 6C is utilized (see [24] for details). The data provided to the observers include the voltage readings at the reference electrode and the collectors, current, and temperature.The observers are initialized with incorrect values of SOC (50% error) and total moles of lithium in the solid and electrolyte phases, 5% and 25% error, respectively. Note that a time step of one second was used in the computation of these results and higher accuracy can be achieved with smaller discretizations.

Figure 3 depicts the current profile of the UDDS drive cycle. The peak of 6-C is higher than those reported in previous studies, which demonstrates the performance of the observer in extreme conditions. Figure 4(b) and 4(c) demonstrate that the Voltage Error Injection (VEI) observer quickly converges to the true voltages of the positive and negative domains with RMS of the error shown in Table II. The total voltage is the sum of the two plots. This result is an improvement of the result in [5], wherein the utilization of a 4C UDDS current yielded an RMS error of 7.4 mV. The observer quickly tracks $c_{ss}^{\pm}(x,t)$ and corrects the initial error in total moles of lithium in the solid phase N_{Ls} as shown in Table III. Note that the error in $c_{ss}^{\pm}(x,t)$ is spatially averaged. Figure 5 displays the normalised $c_s^{\pm}(x,r,t)$ and $z^{\pm}(x,r,t)$, the corresponding error in $c_s^{\pm}(x,r,t)$, at $t^* = 594$ seconds, where the current reaches its maximum during the simulation. This figure shows that the observer system is able to estimate the original system on a spatial level.

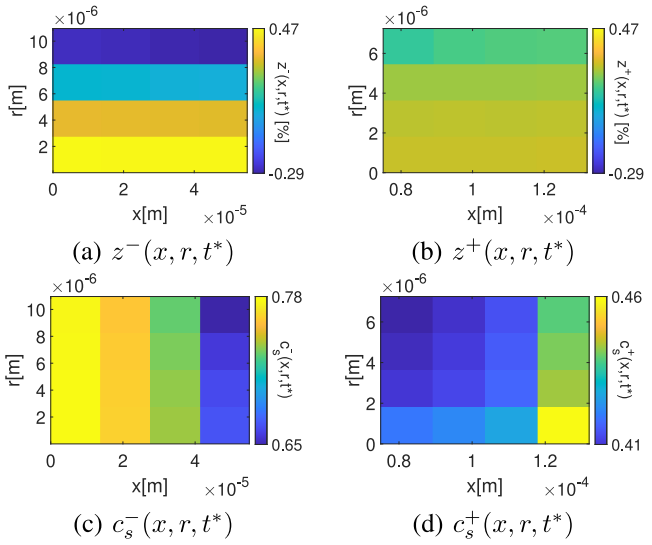

(a) $z^-(x, r, t^*)$ (b) $z^+(x, r, t^*)$

(c) $c_s^-(x, r, t^*)$ (d) $c_s^+(x, r, t^*)$

Fig. 5. $c_s^{\pm}(x, r, t^*)$ and $z^{\pm}(x, r, t^*)$.

TABLE III
RMS VALUE OF PERCENTAGE ERRORS IN $c_{ss}^{\pm}$ AND N_{Ls}

error (%)	c_{ss}^-	c_{ss}^+	N_{Ls}
VEI	0.4717	0.3346	0.0089
VEI (5mV noise)	0.4673	0.3424	0.1657
VEI (10mV noise)	0.5275	0.3791	0.2067

Under the same initial conditions, the robustness of the observer is now tested against voltage noise at the three measurement points of measurement: both collectors and the reference electrode. VEI (5mV noise) signifies a cumulative voltage noise level of 15mV. The RMS values of the voltage and spatially averaged error in $c_{ss}^{\pm}(x, t)$ are presented in Tables II and III, respectively. The observer is able to handle large noise in measurement with little loss in accuracy.

The convergence of the electrolyte observer is now discussed. Simulation results show that after initialization of 200 seconds, the observer quickly converges to the actual value and total moles of lithium in the electrolyte (N_{Le}), with an RMS percentage error of only 0.0269 and 0.0370, respectively. These results confirm the proposed electrolyte observer's reliability and accuracy in tracking the system's state.

V. CONCLUSION

In this letter, we have used information from a reference electrode and the concentration of Li at one point in the electrolyte to propose PDE-based observers for the solid and electrolyte phases of a simplified version of the DFN model of a Li-ion battery. Both observers are proven to be exponentially stable independently, demonstrate accurate tracking of the voltage and concentrations on a spatial level, and show robustness to noise in input voltage measurements. Future work involves the experimental implementation and validation of these observers.

REFERENCES

[1] U. Krewer, F. Röder, E. Harinath, R. D. Braatz, B. Bedürftig, and R. Findeisen, "Dynamic models of Li-ion batteries for diagnosis and operation: A review and perspective," *J. Electrochem. Soc.*, vol. 165, no. 16, 2018, Art. no. A3656.

[2] M.-K. Tran, A. DaCosta, A. Mevawalla, S. Panchal, and M. Fowler, "Comparative study of equivalent circuit models performance in four common lithium-ion batteries: LFP, NMC, LMO, NCA," *Batteries*, vol. 7, no. 3, p. 51, 2021.

[3] Y. Liu, Q. Zhou, and G. Cui, "Machine learning boosting the development of advanced lithium batteries," *Small Methods*, vol. 5, no. 8, 2021, Art. no. 2100442.

[4] M. Doyle, T. F. Fuller, and J. Newman, "Modeling of galvanostatic charge and discharge of the lithium/polymer/insertion cell," *J. Electrochem. Soc.*, vol. 140, no. 6, p. 1526, 1993.

[5] S. J. Moura, F. Bribiesca-Argomedo, R. Klein, A. Mirtabatabaei, and M. Krstic, "Battery state estimation for a single particle model with electrolyte dynamics," *IEEE Trans. Control Syst. Technol.*, vol. 25, no. 2, pp. 453–468, Mar. 2017.

[6] S. Dey and B. Ayalew, "Real-time estimation of lithium-ion concentration in both electrodes of a lithium-ion battery cell utilizing electrochemical–thermal coupling," *J. Dyn. Syst. Meas. Control*, vol. 139, no. 3, 2017, Art. no. 31007.

[7] D. Zhang, S. Park, L. D. Couto, V. Viswanathan, and S. J. Moura, "Beyond battery state of charge estimation: Observer for electrode-level state and cyclable lithium with electrolyte dynamics," *IEEE Trans. Transport. Electrific.*, early access, Jul. 14, 2022, doi: 10.1109/TTE.2022.3191136.

[8] H. Tu, S. Moura, Y. Wang, and H. Fang, "Integrating physics-based modeling with machine learning for lithium-ion batteries," *Appl. Energy*, vol. 329, Jan. 2023, Art. no. 120289.

[9] M. Adaikkappan and N. Sathiyamoorthy, "Modeling, state of charge estimation, and charging of lithium-ion battery in electric vehicle: A review," *Int. J. Energy Res.*, vol. 46, no. 3, pp. 2141–2165, 2022.

[10] X. Wang et al., "A review of modeling, acquisition, and application of lithium-ion battery impedance for onboard battery management," *eTransportation*, vol. 7, Feb. 2021, Art. no. 100093.

[11] S. Tamilselvi et al., "A review on battery modelling techniques," *Sustainability*, vol. 13, no. 18, 2021, Art. no. 10042.

[12] Y. Zhao, P. Stein, Y. Bai, M. Al-Siraj, Y. Yang, and B.-X. Xu, "A review on modeling of electro-chemo-mechanics in lithium-ion batteries," *J. Power Sour.*, vol. 413, pp. 259–283, Feb. 2019.

[13] J. Keil and A. Jossen, "Electrochemical modeling of linear and nonlinear aging of lithium-ion cells," *J. Electrochem. Soc.*, vol. 167, no. 11, 2020, Art. no. 110535.

[14] H. E. Perez, X. Hu, S. Dey, and S. J. Moura, "Optimal charging of li-ion batteries with coupled electro-thermal-aging dynamics," *IEEE Trans. Veh. Technol.*, vol. 66, no. 9, pp. 7761–7770, Sep. 2017.

[15] S. Dey, B. Ayalew, and P. Pisu, "Nonlinear robust observers for state-of-charge estimation of lithium-ion cells based on a reduced electrochemical model," *IEEE Trans. Control Syst. Technol.*, vol. 23, no. 5, pp. 1935–1942, Sep. 2015.

[16] E. Villemin and O. Raccurt, "Optical lithium sensors," *Coordinat. Chem. Rev.*, vol. 435, May 2021, Art. no. 213801.

[17] J. Fleming, T. Amietszajew, E. McTurk, D. P. Towers, D. Greenwood, and R. Bhagat, "Development and evaluation of in-situ instrumentation for cylindrical Li-ion cells using fibre optic sensors," *HardwareX*, vol. 3, pp. 100–109, Apr. 2018.

[18] J. Schwartz et al., "Embedded fiber optic sensors for in situ and in-operando monitoring of advanced batteries," *MRS Online Proc. Library*, vol. 1740, pp. 7–12, Dec. 2014.

[19] P. Harks, F. Mulder, and P. Notten, "In situ methods for Li-ion battery research: A review of recent developments," *J. Power Sour.*, vol. 288, pp. 92–105, Aug. 2015.

[20] L. Meyer, N. Saqib, and J. Porter, "Operando optical spectroscopy studies of batteries," *J. Electrochem. Soc.*, vol. 168, no. 9, 2021, Art. no. 90561.

[21] A. Allam and S. Onori, "An interconnected observer for concurrent estimation of bulk and surface concentration in the cathode and anode of a lithium-ion battery," *IEEE Trans. Ind. Electron.*, vol. 65, no. 9, pp. 7311–7321, Sep. 2018.

[22] S. Dey, Y. Shi, K. Smith, A. M. Colclasure, and X. Li, "From battery cell to electrodes: Real-time estimation of charge and health of individual battery electrodes," *IEEE Trans. Ind. Electron.*, vol. 67, no. 3, pp. 2167–2175, Mar. 2020.

[23] C. Zhang et al., "Real-time estimation of negative electrode potential and state of charge of lithium-ion battery based on a half-cell-level equivalent circuit model," *J. Energy Stor.*, vol. 51, Jul. 2022, Art. no. 104362.

[24] S. J. Moura, J. L. Stein, and H. K. Fathy, "Battery-health conscious power management in plug-in hybrid electric vehicles via electrochemical modeling and stochastic control," *IEEE Trans. Control Syst. Technol.*, vol. 21, no. 3, pp. 679–694, May 2013.